Coordination of pentaammineruthenium to RNA: spectra, equilibria, kinetics and electrochemistry

Maria A. McNamara and Michael J. Clarke*
Department of Chemistry, Boston College, Chestnut Hill, MA 02167 (USA)

(Received January 13, 1992)

Abstract

The reaction of $[H_2O(NH_3)_5Ru]^{2+}$ with a mixture of tyrosine and valine tRNAs is first order in $[P_{RNA}]$ and $[H_2O(NH_3)_5Ru]^{2+}$ with $k=6.0\pm0.9$ M^{-1} s^{-1}. A strong dependence on ionic strength shows ion-pairing to occur during the course of binding. The equilibrium association constant for the binding of $[H_2O(NH_3)_5Ru]^{2+}$ to guanine sites on RNA is $K_{eq}=2.9\times10^3$. Air oxidation results in the coordination of $[(NH_3)_5Ru]^{3+}$. Signature ligand-to-metal charge transfer bands in the spectra of $[(NH_3)_5Ru^{III}]_n$–RNA samples provide evidence for binding to A, G and C residues with their relative intensities varying with $[Ru]/[P_{RNA}]$ in the reaction mixture. Square-wave and cyclic voltammetry revealed two peaks, which are attributed to the $Ru^{III,II}$ couples of Ru–G, and the sum of Ru–A and Ru–C. Consistent with the spectroscopic results, the relative peak currents indicate that $[Ru\text{–}G]_{RNA} > \{[Ru\text{–}A]_{RNA}+[Ru\text{–}C]_{RNA}\}$. The appearance of a new current peak following reduction of $[(NH_3)_5Ru^{III}]_n$–RNA suggests migration of the metal to endocyclic A sites.

Introduction**

Platinum group ions exhibit both mutagenic and chemotherapeutic activities in which the initial lesion is thought to be metal ion binding to the N7 of purine residues on DNA [1–3]. A number of ammineruthenium complexes have shown good antitumor activity [3–6] and some are currently under consideration for new drug development [3, 7–9]. DNA is thought to be the target molecule for ruthenium anticancer drugs and binding of $[(H_2O)(NH_3)_5Ru]^{2+}$ to nuclear DNA followed by air oxidation interferes with transcription [10, 11]. Ruthenium complexes are also useful as nucleic acid probes or reporting agents by providing distinct and easily measured electrochemical and visible spectroscopic signals upon coordination to nucleic acids; moreover, the paramagnetism of Ru(III) induces profound changes in the ^1H NMR spectra of the bases. Since multiple copies of mRNA, rRNA and tRNA exist in substantial abundance during protein synthesis and RNA encompasses approximately 1.1% (5% mRNA, 80% rRNA, 15% tRNA) of the total weight of the cell compared with about 0.25% for DNA [12], coordination to RNA is undoubtedly occurring and may contribute to cell toxicity. At the same concentrations that apparently induce lethal effects in DNA, metal ion attack on any or all of the various RNAs might be expected to have the effect of slowing down, rather than eliminating, protein synthesis. In order to begin an investigation of the possible biochemical implications of ammineruthenium ions ligating to RNA, a characterization of the binding of $[(H_2O)(NH_3)_5Ru]^{2+}$ to RNA has been undertaken.

In helical DNA, $[(H_2O)(NH_3)_5Ru^{II}]^{2+}$ binds first to the N7 of deoxyguanosine and then to sites on A and C residues that are normally unavailable in the center of the helix [13]. When single-stranded DNA is employed, binding to all three residues occurs readily, but with G sites significantly favored. In contrast to DNA, RNA has A-type rather than B-type helices and often exhibits bulges and loop structures consisting of 'single-stranded' regions, which render a different type of binding environment than that typically present in helical DNA [14]. As a simple model for these systems, we have used a mixture of ribonucleic acids from Baker's yeast containing mainly tyrosine and valine acceptors [15]. The use of relatively small tRNAs has the advantage of rapid solubility, while presenting both helical and looped regions for binding. Due to the substantial (~50%) single stranded regions in tRNA and the presence of modified nucleosides, more binding to A and C sites, which are sterically inaccessible in the

*Author to whom correspondence should be addressed.

**Abbreviations: Guo, guanosine; Gua, guanine; Ado, adenosine; Ade, adenine; Cyd, cytidine; Cyt, cytosine; P_{RNA}, RNA-phosphate; Ru_{RNA}, ruthenium bound to RNA; $[Ru]/[P_{RNA}]$, reactant Ru to P_{RNA} ratio; $[Ru_{RNA}]/[P_{RNA}]$, ratio of ruthenium bound to RNA to P_{RNA}.

0020-1693/92/$5.00

interior of double helices, might be expected. Owing to the reducing, hypoxic environment of many tumors 16, 17], it is likely that, *in vivo*, a prototypical complex, such as $[Cl(NH_3)_5Ru^{III}]^{2+}$, would be converted to $[(H_2O)(NH_3)_5Ru^{II}]^{2+}$. Consequently, the latter ion has been used for bonding to RNA; but, due to the facile oxidation of the Ru^{II} complexes in air, isolation and characterization has been carried out in the Ru^{III} form. Binding of the divalent cation $[(H_2O)(NH_3)_5Ru]^{2+}$ to tRNA is shown to occur rapidly and to depend on ionic strength. Its distribution among the bases varies somewhat as a function of relative ruthenium and RNA concentrations ($[Ru]/[P_{RNA}]$).

Experimental

Synthesis

Stock solutions of $[Cl(NH_3)_5Ru^{III}]^{2+}$ were prepared by dissolving 100 mg (0.33 mmol) of its chloride salt with the addition of two equivalents of AgTFA (where TFA = trifluoroacetate) to remove the ionic chloride. The resulting solutions were adjusted to a pH of 3–4 and a final $[Cl(NH_3)_5Ru^{III}]^{2+}$ concentration of approximately 0.03 M. Under these conditions the complex slowly hydrolyzes to yield $[(H_2O)(NH_3)_5Ru^{III}]$; however, this has no effect on the results reported here. Reduction to $[(H_2O)(NH_3)_5Ru^{II}]^{2+}$ was carried out in an argon purged solution over Zn amalgam for 30 min.

$[(NH_3)_5Ru^{III}]_n$–RNA was prepared using RNA (Sigma, Type III) from baker's yeast [15]. Initial RNA solutions were first extracted with phenol/chloroform (1:1) and then with chloroform. Butanol was used to remove any remaining chloroform. Solutions were also incubated with Proteinase K at 37 °C for 24 h. However, since these procedures had little effect on A_{260}/A_{280} or the coordination experiments, later solutions were used directly. Stock solutions of RNA were prepared by dissolving the RNA in TA buffer (40 mM Tris, 5 mM sodium acetate adjusted to pH 7.8 with acetic acid) and diluting to a $[P_{RNA}] = 1.5$ mM. P_{RNA} concentrations were determined spectrophotometrically from A_{260} by using $\epsilon_{260} = 7400\ M^{-1}\ cm^{-1}$ [18]. Ruthenium–RNA complexes were prepared from aliquots of these solutions, which had been purged with argon for 0.5 h and then injected with varying amounts of the $[(H_2O)(NH_3)_5Ru^{II}]^{2+}$ stock solution. Reactions were allowed to proceed for 1 h at room temperature with continuous argon bubbling. Oxidation to yield $[(NH_3)_5Ru^{III}]_n$–RNA was accomplished by a 1 h purge with oxygen, which caused the initially yellow $[(NH_3)_5Ru^{II}]_n$–RNA to turn a red–purple color. Two different procedures were employed to remove unreacted metal ion from freshly prepared samples. (i) At low $[Ru]/[P_{RNA}]$ (less than 0.3), the reactant mixture was placed on a Biorex-70 cation exchange column and the anionic $[(NH_3)_5Ru^{II}]_n$–RNA was eluted with water. (ii) At $[Ru^{II}]/[P_{RNA}] > 0.5$, $[(NH_3)_5Ru^{III}]_n$–RNA increasingly adhered to the top of the cation-exchange column, indicating that sufficient Ru^{III} was coordinated to the nucleic acid to render it cationic, at least in localized regions. Consequently, precipitation of $[(NH_3)_5Ru^{II}]_n$–RNA was performed to effect removal of excess Ru. After adjusting the samples to 0.3 M sodium acetate with 20% sodium acetate, $[(NH_3)_5Ru^{III}]_n$–RNA was precipitated by the addition of 2.5–3.0 volumes of ethanol followed by cooling in a dry ice/acetone bath. The RNA was separated by centrifugation at 0 °C and 12 000 g for 15 min, after which, the pellet was dissolved in TE buffer (10 mM Tris, 1 mM EDTA, pH = 8.0). To assure complete removal of excess metal ion, this procedure was repeated twice more.

Guanosine, adenosine and cytidine (Sigma) were used without further purification. The monomeric complexes: 7-$[(Guo)(NH_3)_5Ru]Cl_2$, 7-$[(Gua)(NH_3)_5Ru]Cl_2$ [19], 7-$[(Ado)(NH_3)_5Ru]Cl_2$, 7-$[(Ade)(NH_3)_5Ru]Cl_2$, 7-$[(Cyd)(NH_3)_5Ru]Cl_2$ and 7-$[(Cyt)(NH_3)_5Ru]Cl_2$ [20] were synthesized by previously reported methods.

Compound characterization

UV and visible absorption spectra were determined on a Cary 2400 spectrophotometer interfaced to an IBM PS/2-55 computer with Spectra Calc™ software. $[Ru_{RNA}]$ was determined on an Instrumentation Laboratory model 551 atomic absorption spectrophotometer with a model 655 furnace atomizer or on a Varian 1475 atomic absorption spectrophotometer with a Varian 95 graphite thermal atomizer with robotic injection system [13, 20]. Standard solutions were prepared from vacuum desiccated $[(NH_3)_6Ru]Cl_3$.

^1H and ^{31}P NMR spectra were recorded on a Varian Unity 300 Fourier transform spectrometer. To remove as much H_2O as possible, samples were dissolved in D_2O, lyophilized in a dry ice/acetone bath and placed in a vacuum desiccator overnight (repeated 3×). Trimethylphosphine was used as an internal standard for ^{31}P NMR.

Cyclic and square-wave voltammetries were performed on an electrochemical apparatus constructed in this laboratory. All measurements were determined in TA or TE buffer. Ionic strengths were adjusted with LiCl or sodium tosylate. The working electrode was carbon paste and a platinum wire served as the counter electrode with Ag/AgCl as the reference electrode. Solutions were purged with argon before measurements were taken. The scan rate was 500 mV/s for cyclic voltammetric scans. Square-wave measurements were made with staircase step size of 2 mV, 2 ms (1.0 V/s) for each staircase plateau and a pulse height of 50

mV. Due to the polymeric nature of the RNA, which apparently lead to adsorption on repetitive scans, it was necessary to use a fresh surface of carbon paste for each scan. Pre-electrolysis (delay time) experiments were performed by waiting at a reducing potential ($E \leqslant -0.275$ V) for increasing amounts of time before scanning positively. $[(Pyr)(NH_3)_5Ru]Cl_2$ (Pyr = pyridine) ($E°=300$ mV) and $[(NH_3)_6Ru]Cl_2$ ($E°=57$ mV) were used as internal standards.

RNA hydrolysis

RNA hydrolysis was effected by sonication in an 85 °C water bath for 1 h after adjusting the sample pH to 1 with HCl. The samples were cooled, adjusted to pH 8 and chromatographed on a Biorex-70 cation exchange column. Alternatively, samples were hydrolyzed with a combination of nuclease S1 and bacterial alkaline phosphatase (US Biochemical Corp.). In a typical hydrolysis 1 μl of each enzyme solution, 20 μl of a 10× buffer (200 mM NaCl/5 mM $MgCl_2$/0.1 mM $ZnSO_4$/25 mM sodium acetate, pH = 5.5) and 178 μl of RNA were combined (final concentrations: 267 units of S1, 0.45 units of phosphatase, $[P_{RNA}] \sim 0.13$ mM) and allowed to stand at room temperature for 1 h. Analytical HPLC was done on a 100×4.6 mm Rainin Microsorb Short-One 3 μm, C_{18} column fitted to a Gilson 111B UV detector set at 254 nm with the solvent pumped at 1.00 ml/min by an IBM LC 9521 Isocratic modular pump. The eluent was 0.25 M propionic acid, adjusted to pH = 7.39 with ammonium hydroxide. All solutions were filtered through a 0.45 μm Millepore filter, degassed and sonicated before use. The system was allowed to equilibrate for 1 h prior to use.

Kinetic measurements

Reaction kinetics of $[(H_2O)(NH_3)_5Ru^{II}]^{2+}$ with RNA were generally run under pseudo-first order conditions with $[Ru^{II}]/[P_{RNA}] \leqslant 0.1$ in TA buffer, pH = 7.8, 25 °C and monitored at 365 nm. Reactant solutions were prepared by purging a solution of $[Cl(NH_3)_5Ru^{III}]^{2+}$ with zinc amalgam under argon, while an RNA solution was deaerated in an argon purged cuvette for 30 min. An aliquot of the Ru^{II} solution was then transferred anaerobically into the cuvette and sealed. Rate constants were determined from least-squares fits of $\ln(A_\infty - A_t)$ versus time over their linear portion (at least two half-lives). While reactions were run in cuvettes sealed under argon, some reactions revealed the presence of oxygen by a slight color change from light yellow to a red–purple color and a decrease in absorbance at 365 nm over 1 h. Initial rates were determined from the change in absorbance versus time over the first ~5% of the reaction.

Equilibrium binding

To determine the amounts of metal binding to G, A and C sites, spectra of samples of $[(NH_3)_5Ru^{III}]_n$–RNA prepared as above were recorded and their absorbances at three wavelengths analyzed using the following simultaneous equations

$$A_{471} = 6990[\text{Ru–C}] + 3500[\text{Ru–A}] + 150[\text{Ru–G}]$$

$$A_{532} = 1710[\text{Ru–C}] + 5600[\text{Ru–A}] + 310[\text{Ru–G}]$$

$$A_{560} = 386[\text{Ru–C}] + 4420[\text{Ru–A}] + 600[\text{Ru–G}]$$

Equilibrium covalent binding constants (K_{assoc}) for binding to G sites were calculated from a least-squares fit to the Scatchard Equation:

$$\frac{[\text{Ru–G}_{RNA}]}{[G_{RNA}]} = \frac{R_{max} K_{assoc} [Ru]}{1 + K_{assoc}[Ru]}$$

where $[G_{RNA}]$ is the concentration of G sites in the RNA ($[G_{RNA}] = 0.27[P_{RNA}]$), [Ru], is the concentration of uncoordinated ruthenium calculated as the difference between the total ruthenium concentration and that bound to RNA ($[Ru] = [Ru]_0 - [\text{Ru–RNA}]$), and R_{max} is the maximum fraction of G sites available for coordination.

Results

Compound characterization

Typically, ~30 min after the injection of $[(H_2O)(NH_3)_5Ru^{II}]^{2+}$ into RNA solutions, a broad absorbance in the near-UV portion of the spectrum (350–400 nm) was observed. Since $[L(NH_3)_5Ru^{II}]^{2+}$ (L = Guo, Ado, Cyd) all absorb in this region [19, 20], sufficient spectroscopic resolution does not exist to quantitate the amount of binding to each. Typically there was an initially rapid increase in A_{365} with reaction time followed by a gradual, but continued, increase in absorption, whose slope increased with increasing $[Ru^{II}]/[P_{RNA}]$. Figure 1 illustrates a typical series of UV–Vis spectra of $[(NH_3]_5Ru^{III}]_n$–RNA samples run at varying $[Ru^{II}]/[P_{RNA}]$ following a reaction time of 1 h and air oxidation. As $[Ru^{II}]/[P_{RNA}]$ increases from 0.1 to 1.0, the color of the oxidized reaction mixture increases with a shift in the absorption maximum to higher energy. Reaction ratios higher than 1.0 caused a brown precipitate to form upon oxidation. Figure 2 shows the average amounts of Ru^{II} binding to A, G and C sites as a function of $[Ru^{II}]/[P_{RNA}]$ as determined by spectrophotometric analysis [19, 21].

When the samples were allowed to stand at room temperature after three ethanol precipitations had been performed, some gradually turned a brown color and eventually precipitated over the period of 2–3 days, suggesting that not all the excess ruthenium had been

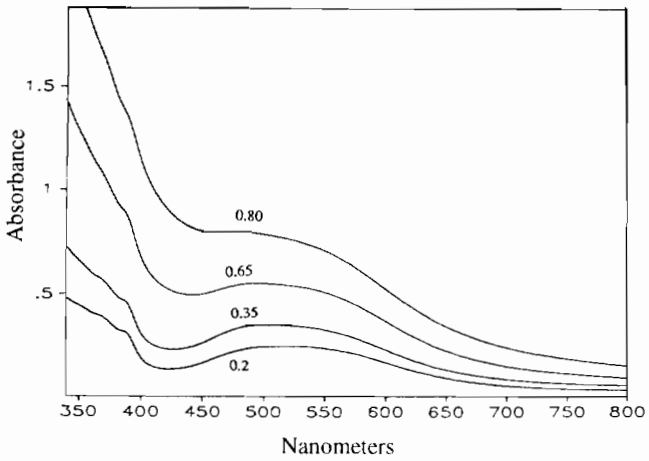

Fig. 1. Typical absorption spectrum of $[(NH_3)_5Ru^{III}]_n$–RNA samples from reaction run at $[Ru^{II}]/[P_{RNA}]=0.2$, 0.35, 0.65, 0.80 and $[P_{RNA}]=1.5$ mM. Samples were oxidized for 1 h by O_2 sparging.

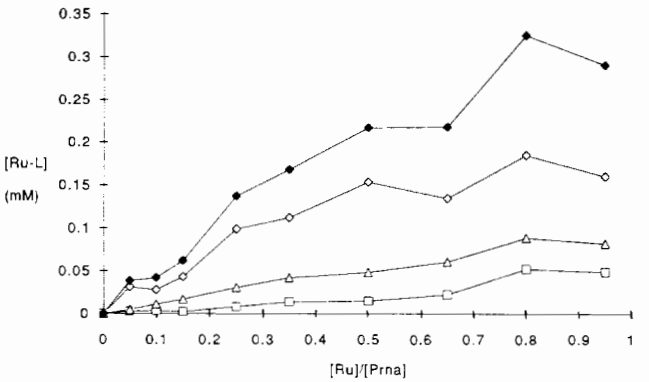

Fig. 2. Relative concentrations (mM) of ruthenium(III) binding to A, G and C sites as a function of $[Ru^{II}]/[P_{RNA}]$ at $[P_{RNA}]=1.5$ mM as determined from spectrophotometric analyses of oxidized solutions of $[(NH_3)_5Ru^{III}]_n$–RNA. ◆, $[Ru\text{–}RNA]_{total}$; ◇, [Ru–Guo]; △, [Ru–Ado]; □, [Ru–Cyd].

removed. Similar discoloration had not been observed with $[(NH_3)_5Ru^{III}]_n$–DNA (helical or single-stranded) [13]. To overcome this difficulty an ion-exchange method was used to separate unreacted ruthenium at the lower $[Ru^{II}]/[P_{RNA}]$, where the problem appeared most acute on the basis of atomic absorption determinations of $[Ru_{RNA}]/[P_{RNA}]$. Since unreacted ruthenium does not interfere with the UV–Vis spectrophotometric analysis, which depends on charge-transfer bands well removed from the reactant material and its oxidized products, reliance is placed on the spectrophotometric data, which is base specific, rather than the atomic absorption results, which reflect total $[Ru_{RNA}]/[P_{RNA}]$. However, total $[Ru_{RNA}]/[P_{RNA}]$ corresponded fairly well between the two analytical methods.

$[(NH_3)_5Ru^{III}]_n$–RNA prepared at $[P_{RNA}]=3.99$ mM and $[Ru]=0.9975$ mM ($[Ru^{II}]/[P_{RNA}]=0.25$ yielded a ^{31}P NMR resonance (25 °C, pH = 8.0) at −4.069 ppm with a broader linewidth ($w_{1/2}=190$ Hz) compared with uncomplexed RNA which exhibited a resonance at −3.898 ppm ($w_{1/2}=89$ Hz) relative to trimethylphosphine.

Electrochemistry

Current peak potentials are summarized in Table 1 along with the potentials for $[L(NH_3)_5Ru^{III,II}]$, where L = guanosine, adenosine and cytidine. Since the potentials for the latter two complexes are similar, peak currents simultaneously arising from coordination to both sites on RNA cannot be resolved. A typical cyclic voltammetry scan of $[(NH_3)_5Ru^{III}]_n$–RNA is shown in Fig. 3(a). In order to obtain a good signal, it was necessary to use samples prepared at $[Ru^{II}]/[P_{RNA}]=0.75$, $[P_{RNA}]=3.45$ M, which is on the border of the precipitation limit. The largest peak current occurs at 56 mV, which is in the range expected for $[(Guo)(NH_3)_5Ru]^{3+}$ (cf. Table II, ref. 19). The separation between the anodic and cathodic cyclic voltammetric peaks was 58 mV, which is consistent with a single-electron transfer process. An irreversible peak at −170 mV was observed and is in the range expected for the reduction of exocyclically coordinated $[(Ado)(NH_3)_5Ru]^{3+}$ and $[(Cyd)(NH_3)_5Ru]^{3+}$ [20]. When probed by the more sensitive and higher resolution square-wave technique (Fig. 3(b)), the same current peaks were observed. Potentials for both peaks varied linearly with $\sqrt{\mu}$ and $\log(\mu)$. In the case of guanine, the slope was 70.5 ± 7 mV/$\sqrt{\mu}$ while for the {A+C} peak the corresponding values are 114 ± 18 mV/$\sqrt{\mu}$.

The voltammetric peak heights at $[Ru]/[P_{RNA}]$ less than 0.7 were approximately 1.5 times greater for L = G relative to L = {Ado + Cyd}. While the electrochemical and spectroscopic studies are consistent in showing that coordination to guanosine sites predominates, absorption effects prohibit precise quantitation in the former. Although coordination of Ru^{III} is mainly to the excocyclic positions on Ado and Cyd, holding at a reducing potential for increasing lengths of time yields a new peak at 300 mV versus NHE, which is indicative of

TABLE 1. Summary of current peak potentials of $[(NH_3)_5Ru^{III}]_n$–RNA along with the potentials for $[L(NH_3)_5Ru^{III,II}]$, where L = guanosine, adenosine and cytidine

Ligand	Probable binding site	E_f vs. NHE (mV)	RNA[d] E_f vs. NHE (mV)
Cytidine	N4	−196[a]	−175
Adenosine	N6	−170[c]	
Adenosine	N1	325[c]	405
G-Nucleic acid	N7	48[b]	56

[a]From ref. 22; corrected to pH = 8.0, $\mu=0.1$. [b]From ref. 23; buffer at pH = 7.8, $\mu=0.044$. [c]From ref. 24; $\mu=0.1$. [d]Average of several trials in TE buffer at pH = 8.0, $\mu=0.045$.

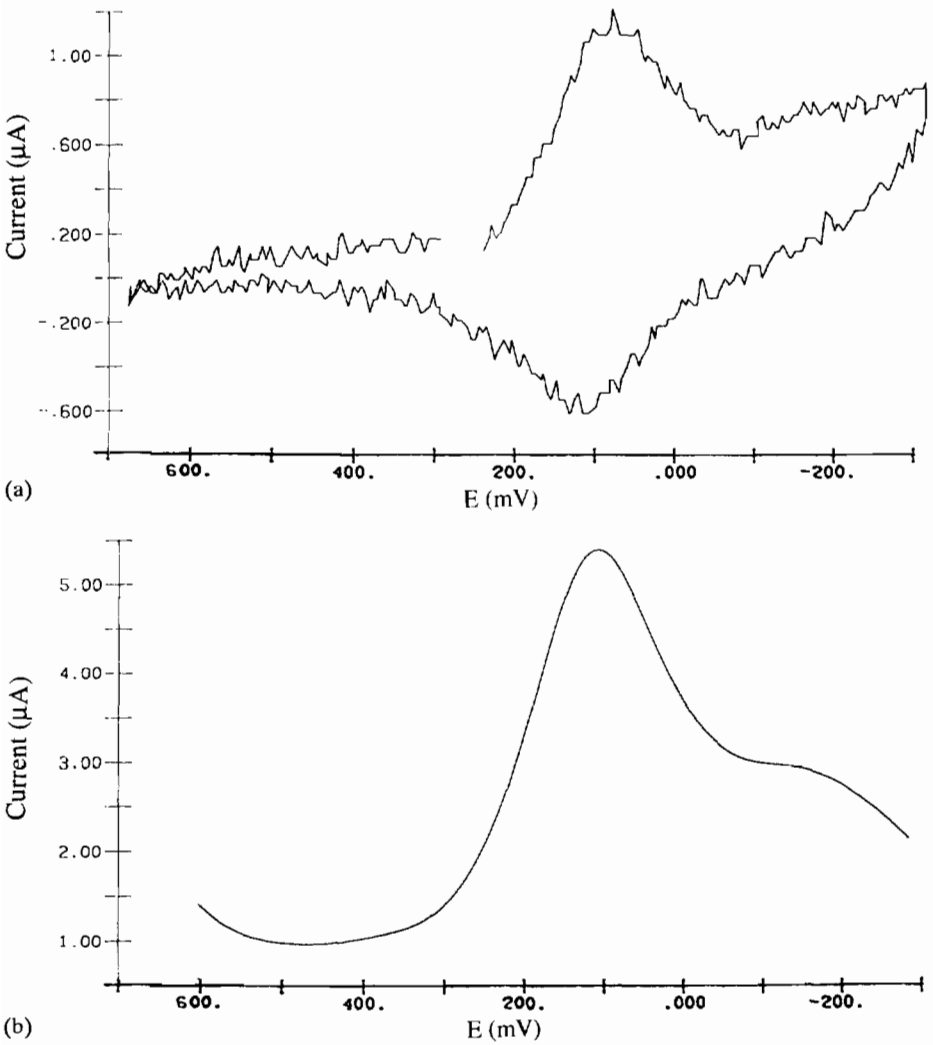

Fig. 3. (a) Cyclic voltammogram of $[(NH_3)_5Ru^{III}]_n$–RNA in TA buffer. $[Ru^{II}]/[P_{RNA}]=0.75$, $[P_{RNA}]=1.5$ mM. (b) Square-wave voltammogram of the same solution.

binding of Ru^{II} to the endocyclic (N1) site of adenosine (Fig. 4). [20].

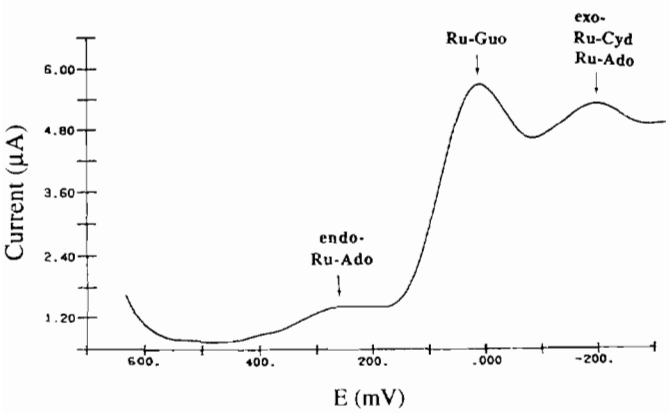

Fig. 4. Square-wave voltammogram of $[(NH_3)_5Ru^{III}]_n$–RNA; $[Ru^{II}]/[P_{RNA}]$-0.50, $[P_{RNA}]=1.5$ mM, holding at −500 mV for 5000 ms and then scanning cathodically.

Hydrolysis of $[(NH_3)_5Ru^{III}]_n$–RNA

A combination of S1 exonuclease, which hydrolyzes single-stranded nucleic acids, and bacterial alkaline phosphatase, which cleaves the phosphodiester bond, was used to lyse $[(NH_3)_5Ru^{III}]_n$–RNA samples. A comparison of HPLC retention times of: (i) hydrolyzed $[(NH_3)_5Ru^{III}]_n$–RNA, (ii) hydrolyzed RNA, and (iii) nucleoside standards showed that the $[(NH_3)_5Ru^{III}]_n$–RNA was largely broken down to monomeric, uncoordinated nucleosides, with small peaks arising from the modified nucleosides. Additional smaller peaks evident in the chromatogram of hydrolyzed $[(NH_3)_5Ru^{III}]_n$–RNA may be due to di- or oligonucleotides arising from inefficient enzymatic cleavage. Comparison of peak heights from a sample run at $[Ru]/[P_{RNA}]=0.25$ indicated that the guanosine peaks of the ruthenated samples were 48% smaller than those of the native RNA, while the other three nucleoside peaks were unchanged within experimental error. While

a small peak corresponding to $[Guo(NH_3)_5Ru]^{3+}$ was present in these HPLCs, it was not sufficiently intense to yield a signal when monitored at 550 nm, a region in which the guanosine complex exhibits a broad (but not intense) absorption.

Hydrolysis of $[(NH_3)_5Ru^{III}]_n$–RNA was also attempted with heating and sonication at low pH (85 °C, pH 1.0, 1 h). After adjusting the pH back to 8.0, a number of bands were resolved on a Biorex-70 cation exchange column. The spectra of the three largest bands, which eluted with 0.6, 0.6 and 0.8 M ammonium formate, respectively, exhibited maxima at 552, 545 and 512 nm, respectively. While the spectra were similar to 6-$[Ado(NH_3)_5Ru^{III}]$ and 7-$[Guo(NH_3)_5Ru^{III}]$, comparison of the HPLC retention times of these fractions with those of the known Ru–nucleoside and Ru–purines, showed that they were not simple, monomeric adducts. Since heat-induced crosslinking to a second guanosine site was a possibility, 7-$[Guo(NH_3)_5Ru^{III}]$ was heated with a two-fold excess of 5′-GMP and a similar increase in intensity and bathochromic shift was observed. Ion exchange analysis on DEAE-Sephadex (anion-exchange resin) and Biorex-70 (cation-exchange resin) revealed the complex to be anionic, indicating coordination of the GMP, probably in a *trans* position owing to steric effects. Following rotary evaporation of the chromatographic fraction, a dark purple residue was obtained; however, this material would not redissolve in a reasonable amount of water or organic solvents.

Kinetics

Since the second phase of the reaction, which increased with $[Ru]/[P_{RNA}]$, was substantially slower than the first and extended into periods where air leakage and possibly ammine substitution became possibilities, only the more rapid and reproducible first phase of binding is treated. Limits imposed by metal ion precipitation of the RNA and the need for adequate absorbance changes restricted the range of reactant concentrations available. Plots k_{obs} versus $[P_{RNA}]$ obtained under pseudo-first order conditions (Fig. 5(a)) and of initial rates versus [Ru] (Fig. 5(b)) were both linear. The former yielded a second order rate constant of $5.96 \pm 0.94\ M^{-1}\ s^{-1}$.

When the ionic strength was adjusted with LiCl a plot of $\log(k_{obs})$ versus $\sqrt{\mu}$ yielded a slope of -2.21; however, when sodium tosylate was used, a value of -2.07 was obtained as shown in Fig. 6.

Equilibria of binding

Samples in which the binding of $[(H_2O(NH_3)_5Ru]^{2+}$ to RNA had essentially reached equilibrium after the rapid phase of the coordination reaction was complete were quenched by oxidation. However, at longer times and higher $[Ru]/[P_{RNA}]$, small and varying amounts of the secondary reaction had also occurred. While the concentration of ruthenium binding to G, A and C residues was determined by spectrophotometric methods, coordination to exocyclic ammines of the latter occurs upon oxidation, while in the case of guanine, binding has already occurred and only the oxidation state is altered by oxidation. Consequently only the equilibrium binding constant for binding to G sites on RNA can be estimated from spectrophotometric data, which is plotted in the form of a Scatchard plot in Fig. 7 and yields $K_{assoc} = (2.9 \pm 0.9) \times 10^3$ with $R_{max} = 0.6$.

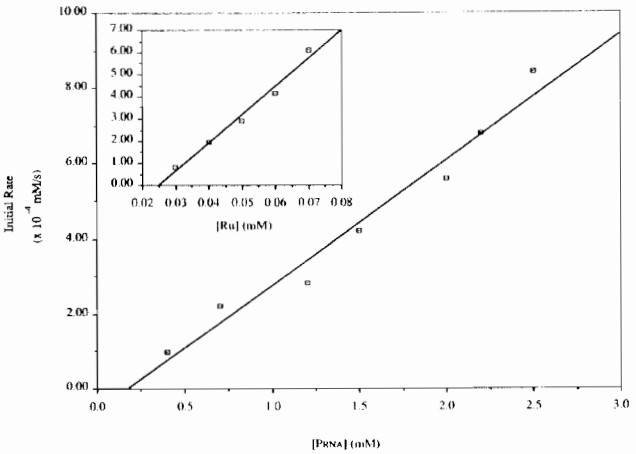

Fig. 5. (a) Plot of k_{obs} for the binding of $[(H_2O(NH_3)_5Ru]^{2+}$ to RNA at varying $[P_{RNA}]$ in TA buffer at $\mu = 0.040$, pH = 7.8 and 25 °C. Each point represents an average of three runs. (b) Inset: plot of initial rates of binding of $[(H_2O)(NH_3)_5Ru]^{2+}$ to RNA at varying $[Ru^{II}]$ at $[P_{RNA}] = 2.8$ mM TA buffer at $\mu = 0.040$, pH = 7.8 and 25 °C. Each point represents an average of three runs.

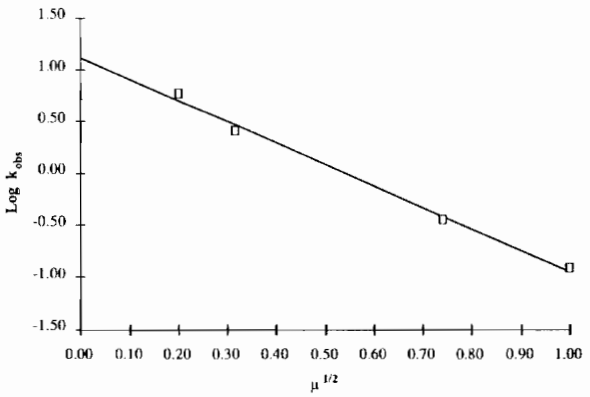

Fig. 6. Plot of $\log(k_{obs})$ vs. $\sqrt{\mu}$ in TA buffer with ionic strength adjusted with sodium tosylate.

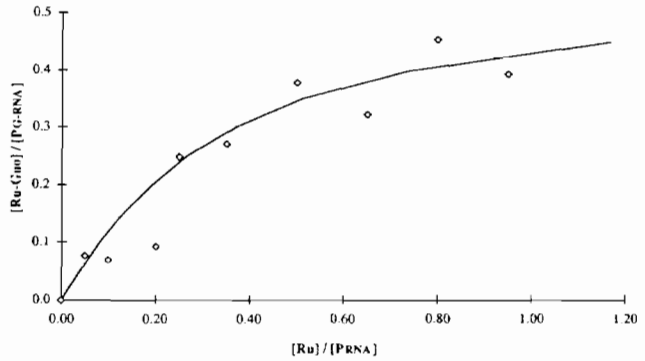

Fig. 7. Scatchard plot of $[Ru\text{–}G_{RNA}]/[G_{RNA}]$ versus $[Ru^{II}]/[P_{RNA}]$.

Discussion

Compound characterization

Since phosphates and uridine and cytidine nucleosides do not react with $[(H_2O)(NH_3)_5Ru^{II}]^{2+}$ under these conditions to yield stable complexes [13], the increase in absorbance in the 350–400 nm region can be attributed to purine complexation by the metal ion [13]. The slower, second phase rise in absorbance is probably due to additional adenosine binding following localized unwinding of the RNA. In monomeric compounds, coordination to the exocyclic amine sites of A and C occurs upon oxidation. In the case of adenosine, this appears to be largely intramolecular following Ru^{II} coordination to N1 [21]. With cytidine, steric hindrance to endocyclic coordination at N3 suggests that binding to this site is more transient, if it occurs at all. Consequently, coordination to cytosine residues takes place largely in the oxidation step under non-equilibrium conditions.

Since the intensities of the visible LMCT bands of the adenosine ($\epsilon \approx 5.6\times10^3$ M^{-1} cm^{-1}) and cytidine ($\epsilon = 6.99\times10^3$ M^{-1} cm^{-1}) complexes are significantly greater than the guanosine band ($\epsilon \approx 0.441\times10^3$ M^{-1} cm^{-1}), they are more evident in the spectra of $[(NH_3)_5Ru^{III}]_n$–RNA. However, when the relative concentrations of metal binding to each of these bases is calculated or when estimated from the square-wave peak heights, it is evident that there is more binding to guanosine than adenosine and cytidine (cf. Figs. 1–3). The relative increase in cytidine binding as $[Ru^{II}]/[P_{RNA}]$ increases may have to do with easing the steric hindrance to attack at the N4 site on unfolding the RNA structure as more of the metal ion coordinates.

The mixture of tRNAs is approximately 27% guanosine type bases, 21% adenosine type and 27% cytidine type. At the highest ratio, about 56% of the guanosine type residues coordinate compared to about 24% of adenosine and 18% of cytidine type residues. Since increased Ru binding neutralizes the polyanionic charge on the RNA, at $[Ru^{II}]/[P_{RNA}]$ ratios >1.0 precipitation occurs. At reactant ratios below 0.1 essentially all of the binding is to the N7 of guanosine type residues (cf. Fig. 2).

Rubin *et al.* [25] investigated the binding of *cis*-$[Pt(NH_3)_2Cl_2]$, *trans*-$[Pt(NH_3)_2Cl_2]$ and $[Cl(NH_3)_5Ru]^{3+}$ to yeast phenylalanine tRNA by X-ray crystallography and found that binding of these complexes occurred mainly in regions where guanosine N7 sites were well exposed and the negative phosphate charge density was the highest. While these workers allowed solutions of $[Ru(NH_3)_5Cl]Cl_2$ to soak into crystals of $tRNA^{phe}$ for unusually long reaction times (25 and 58 days), their results have some relevance here in explaining why unreacted Ru^{III} was more difficult to remove from RNA than DNA. The crystallographic study showed that Ru^{III} cations have a high affinity for looped regions, which concentrate phosphate negative charge. Under the conditions reported here, strong electrostatic forces may bind Ru^{III} sufficiently well as to render it unremovable by ethanol precipitation of the RNA. As the reactant ratio is increased and more charged ruthenium complexes are added to reduce the anionic charge and disrupt the structure of the nucleic acid, this tendency should decrease.

Electrochemistry

As expected, the potential of the largest electrochemical peak, which is attributed to $[G(NH_3)_5Ru^{III,II}]_n$–tRNA, is close to that obtained with helical DNA (Table 1). The peak width for this couple (see Figs. 3 and 4) is appreciably larger than that for $[Guo(NH_3)_5Ru^{III,II}]$ (180 mV) which may be due to the adjacent overlapping peaks and diffusion differences between the polymer and monomer complexes. On the basis of the spectroscopic evidence and by analogy to the reduction potentials of the monomeric complexes [21], the peak at -170 mV is attributed to a combination of $[A(NH_3)_5Ru^{III,II}]_n$–tRNA and $[C(NH_3)_5Ru^{III,II}]_n$–tRNA. The increase in reduction potentials with the square root of the ionic strength indicates that the effect of the negative charge on the phosphate backbone is less efficient in stabilizing Ru^{III} over Ru^{II} as other cations become available to interact with the anionic phosphates. This may be due either to a difference in ion-pairing between the oxidized and reduced forms, or simply to the relative change in activity coefficients as a function of ionic strength. Derivations of the various possible cases are given in the Appendix. Since the slope of E versus $\sqrt{\mu}$ is greater for the $Ru^{III,II}$–A line than for the $Ru^{III,II}$–G, it appears that the slope is dependent on the net effective charge on the metal complex, which is most consistent with

an effect generated by the relative change in activity coefficients as a function of ionic strength.

The increase in the square-wave current at 400 mV, with increasing reduction times (Fig. 5), indicates the formation of a new species. A similar phenomenon is seen in the electrochemistry of 6-[Ado$(NH_3)_5Ru^{III}$], in which the metal ion is thought to migrate from the exocyclic nitrogen (N6) to the adjacent ring nitrogen site (N1) [21]. The potential of 1-[Ado$(NH_3)_5Ru^{III,II}$] is 325 mV, which is less than what is observed on tRNA. This suggests that the relative stability of the endocyclic binding site for Ru^{II} is somewhat higher than in the monomer, which could arise from the RNA bases forming a lower dielectric region around the metal ion than occurs in the bulk, aqueous solution.

The analogous linkage isomerization is not seen with cytidine as a ligand, since the ring nitrogen is sterically hindered. Consequently, the increased peak current around 400 mV strongly suggests a migration of the metal ion to adenosine N1 sites. However, as there are three reservoirs of the metal ion (on guanosine and cytidine as well as adenosine), and the square-wave results are not sufficiently sensitive to indicate a clear decrease in either the Ru–Guo or {Ru–Ado + Ru–Cyd} peaks, the migration to N1 may come from any of the possible sources.

Hydrolysis and HPLC

Exposure to very high pH causes ruthenium ammine complexes to undergo hydrolysis, oxidation and oligomerization; consequently, this method of lysing RNA could not be used. The combined exonuclease and phosphatase hydrolysis of $[(NH_3)_5Ru^{III}]_n$–RNA yielded free nucleosides, which upon quantitation by HPLC revealed that the guanosine peak decreased relatively more in comparison with those for A and C from native RNA samples subjected to the same hydrolytic technique. This is consistent with ruthenium coordination interfering with the enzymic function so as to leave regions around the Ru uncleaved.

The combined effects of heat, acid and sonication also cleaved the $[(NH_3)_5Ru^{III}]_n$–RNA reproducibly into three colored fractions. Since these could be resolved on a cation exchange column, they can be presumed to be of relatively small oligomers in which the charge of the metal ion predominates over any remaining phosphates. Heating [(Guo)$(NH_3)_5Ru^{III}$] with a two-fold excess of 5′GMP ligand yielded a similar increase in absorbance around 570 nm, so that an analogous compound is apparently formed; however, this has proved intractable to isolation and characterization. The base-catalyzed, ruthenium assisted autoxidation of coordinated dG and Guo to give their 8-oxo derivatives [26] was not observed with $[(NH_3)_5Ru^{III}]_n$–RNA, which is consistent with a similar negative result with $[(NH_3)_5Ru^{III}]_n$–DNA [13].

Equilibria of binding

The pentaammineruthenium ion is compact compared to complexes with aromatic ligands of sufficient size to intercalate or provide shape-selectivity [27–30]. Consequently, smaller differences in binding arising from steric constraints are expected between the folded, helical and open regions of tRNA. This allows for an overall approximate binding constant to be obtained for the guanine residues. As indicated previously, binding to cytidine residues is probably redox catalyzed and not at equilibrium [13]. While binding to the N1 of adenosine has probably reached equilibrium with respect to the few sterically accessible sites, continued, but slower, coordination can be expected as the RNA gradually unfolds under the influence of metal ion coordination.

The kinetic studies indicate that binding to guanine sites have reached at least a pseudo equilibrium. The approximate equilibrium binding constant for G^7 sites is somewhat lower than for either double helical (5.1×10^3) or single-stranded (7.8×10^3) DNA [13]. This may have to do with the inherently lower affinity of Lewis acids for ribonucleosides relative to nucleosides (often around a factor of 2–4 in K_as) [31], which arises from the greater electron-withdrawing ability of the ribose's 2′-hydroxyl. Also, the G^7 sites lie much deeper in the major groove of the A-helix of RNA than in the B-helix of DNA, which would lower their affinity for the ruthenium on a steric basis until the helix opens through a denaturing process.

Kinetics

Since the rate decreases markedly with increasing ionic strength, the mechanism probably involves ion-pairing between the metal ion and the nucleic acid in a simple pre-equilibrium fashion. Using the simplest form of this mechanism, the rate law becomes:

$$\frac{d[Ru\text{–}RNA]}{dt} = k_2K_{ip}[Ru^{II}][P_{RNA}] = k_{obs}[Ru^{II}][P_{RNA}]$$

According to Manning theory, increasing the ionic strength should substantially decrease k_{obs} by lowering K_{ip} [32, 33]. However, the slope (-1.27) of a plot of $\log(k_{obs})$ versus $\log(\mu)$ is somewhat less than the value of -2.0 predicted by this theory. The ionic strength dependence agrees well with Debye–Hückel theory in that a plot of $\log(k_{obs})$ versus $\sqrt{\mu}$ (Fig. 6) yields a slope of -2.06, which compares well with the theoretical slope of -2.036 calculated for a dispositive ion interacting with a monoanion [34]. Correlations with either theory are consistent with ion-pairing; however, the

closer correlation with the Debye–Hückel equations suggests that the tRNA is not sufficiently large to behave as the long cylindrical molecule assumed in the Manning treatment. When extrapolated to $\mu=0$, $k_0=13.6\ M^{-1}\ s^{-1}$, which is at the upper limit of the water exchange rate on $[(H_2O)(NH_3)_5Ru]^{2+}$ and indicates that ion-pairing between the metal complex and the RNA greatly facilitates coordination to the bases. Under the same conditions (25°, $\mu=0.045$ M, $[P_{RNA}]=1.5$ mM) the rate of binding to tRNA is 2.7 times faster than to helical DNA, which, at least in part, may be attributed to the more open structure of tRNA caused by the presence of single-stranded regions. However, binding to RNA is still 1.6 times faster than to single-stranded DNA, which suggests that other factors also make RNA binding more rapid than DNA.

Acknowledgements

This work was supported by PHS Grant GM26390. We thank Professor S. J. Lippard (MIT) for generously providing access to the AA apparatus and Mr M. Keck for assistance with these measurements.

References

1 M. Nicolini (ed.), *Platinum and Other Metal Coordination Compounds in Cancer Chemotherapy,* Martinus Nijhoff, Boston, MA, 1987.
2 W. I. Sundquist and S. J. Lippard, *Coord. Chem. Rev., 100* (1990) 293.
3 M. J. Clarke (ed.), *Ruthenium and Other Non-Platinum Metal Complexes in Cancer Chemotherapy,* Vol. 10, Springer, Heidelberg, 1989.
4 M. J. Clarke, *Met. Ions Biol. Syst., 11* (1980) 231–283.
5 M. J. Clarke, in A. E. Martell (ed.), *Inorganic Chemistry in Biology and Medicine,* Vol. 190, American Chemical Society, Washington, DC, 1980, pp. 157–180.
6 M. J. Clarke, in S. J. Lippard (ed.), *Chemistry and Biochemistry of Platinum, Gold and Other Chemotherapeutic Agents,* ACS Symposium Series No. 209, American Chemical Society, Washington, DC, 1983, pp. 335–354.
7 B. K. Keppler, M. R. Berger and M. E. Heim, *Cancer Treat. Rev., 17* (1990) 261–277.
8 S. Pacor, E. Luxich, V. Ceschia, G. Sava, E. Alessio and G. Mestroni, *Pharmacol. Res., 21* (Suppl. 1) (1989) 127–128.
9 E. Alessio, G. Mestroni, G. A. Nardin, M. Wahib, M. Calligaria, G. Sava and S. Zorzet, *Inorg. Chem. 27* (1988) 4099–4106.
10 K. A. Marx, R. Kruger and M. J. Clarke, *Mol. Cell. Biochem., 86* (1989) 155–162.
11 K. A. Marx, C. Seery and P. Malloy, *Mol. Cell. Biochem., 90* (1989) 37–95.
12 B. Alberts, D. Bray, J. Lewis, M. Raff, K. Roberts and J. D. Watson, in *Molecular Biology of the Cell,* Garland, New York, 1983, p. 92.
13 M. J. Clarke, B. Jansen, K. A. Marx and R. Kruger, *Inorg. Chim. Acta, 124* (1986) 13–28.
14 D. Voet and J. G. Voet, in *Biochemistry,* Wiley, New York, 1989, pp. 852–947.
15 R. W. Holley, J. Apgar, B. P. Doctor, J. Farrow, M. A. Marini and S. H. Merrill, *J. Biol. Chem., 236* (1961) 200.
16 P. Vaupel, F. Kallinowski and P. Okunleff, *Cancer Res., 49* (1989) 6449–6665.
17 P. Vaupel, K. Schlenger and C. Knoop, *Cancer Res., 51* (1991) 3316.
18 D. Freifelder, in *Physical Chemistry, Applications to Biochemistry and Molecular Biology,* W. H. Freeman, San Francisco, CA, 1976, p. 384.
19 M. J. Clarke and H. Taube, *J. Am. Chem. Soc., 96* (1974) 5413–5419.
20 M. J. Clarke, M. Buchbinder and A. D. Kelman, *Inorg. Chim. Acta, 27* (1978) L87–L88.
21 M. J. Clarke, *J. Am. Chem. Soc., 100* (1978) 5068–5075.
22 M. J. Clarke, *J. Am. Chem. Soc., 100* (1978) 5068.
23 M. J. Clarke, B. Jansen, K. A. Marx and R. Kruger, *Inorg. Chim Acta, 124* (1986) 13–28.
24 R. Galang, unpublished results.
25 J. R. Rubin, M. Sabat and M. Sundarlingam, *Nucleic Acid Res., 11* (1983) 6571.
26 K. C. Gariepy, M. A. Curtin and M. J. Clarke, *J. Am. Chem. Soc., 111* (1989) 4947–4952.
27 A. M. Pyle, E. C. Long and J. K. Barton, *J. Am. Chem. Soc., 111* (1989) 4520–4522.
28 M. R. Kirshenbaum, R. Tribolet and J. K. Barton, *Nucleic Acid Res., 16* (1988) 7943–7960.
29 D. S. Sigman, *Biochemistry, 29* (1990) 9097–9105.
30 X. Chen, C. J. Burrows and S. E. Rokita, *J. Am. Chem. Soc., 113* (1991) in press.
31 J. H. Lister, in *Fused Pyramidines Part 2: Purines,* Vol. 24, Wiley–Interscience, New York, 1971, pp. 481–494.
32 G. S. Manning, *Q. Rev. Biophys., 11* (1978) 179.
33 X. Hui, N. Gresh and B. Pullman, *Nucleic Acid Res., 18* (1990) 1109.
34 P. W. Atkins, *Physical Chemistry,* W. H. Freeman, San Francisco, CA, 1st edn., 1978, pp. 314–323, 914–817.

Appendix

Variation of reduction potentials with ion concentration

For a simple one electron reduction process, the Nernst equation expressed with activity coefficients has the form

$$e^- + M^{n+} \rightleftharpoons M^{(n-1)+}$$

$$E = E^\circ - \frac{RT}{nF} \ln\left(\frac{\gamma_{(n-1)}[M^{(n-1)+}]}{\gamma_n[M^{n+}]}\right)$$

$$E = E^\circ - \frac{RT}{nF} \ln\left(\frac{[M^{(n-1)+}]}{[M^{n+}]}\right) - 0.059\{\log \gamma_{(n-1} - \log \gamma_n\}$$

Since $\log(\gamma) = -Az_i^2\sqrt{\mu}$, the last term becomes

$$-0.509\{(n-1)^2 - n^2\}\sqrt{\mu} = -0.509(n^2 - 2n + 1 - n^2)\sqrt{\mu}$$
$$= -0.509(-2n+1)\sqrt{\mu} = +2\times 0.509(n-0.5)\sqrt{\mu}$$

and

$$E = E^\circ - \frac{RT}{nF}\ln\left(\frac{[M^{(n-1)+}]}{[M^{n+}]}\right) - 0.059 \times 1.018(n-0.5)\sqrt{\mu}$$

$$E = E^\circ - \frac{RT}{nF}\ln\left(\frac{[M^{(n-1)+}]}{[M^{n+}]}\right) - 0.060(n-0.5)\sqrt{\mu}$$

If M is an anion, M^{n-}, with ion-pairing to an inert cation, then the last term becomes

$$-0.509\{(n+1)^2 - n^2\}\sqrt{\mu} = -0.509(n^2+2n+1-n^2)\sqrt{\mu}$$
$$= -0.509(2n+1)\sqrt{\mu} = -2\times 0.509(n+0.5)\sqrt{\mu}$$

$$E = E^\circ - \frac{RT}{nF}\ln\left(\frac{[M^{(n-1)+}]}{[M^{n+}]}\right) + 0.060(n+0.5)\sqrt{\mu}$$

The variation in potential depends on the charge of the oxidized species:

n	Slope ($mV/\sqrt{\mu}$)	n	Slope ($mV/\sqrt{\mu}$)
1	−30	−1	90
2	−90	−2	150
3	−150	−3	210

When ion-pairing occurs in the oxidized state (cation) and not in the reduced state (neutral) the reduction potential varies as $-\ln(a_X)$ [A1].

$$X^- + M^+ \rightleftharpoons (X\cdot M)K_{ox} = \frac{\gamma[X\cdot M)]}{\gamma_x[X^-]\gamma_+[M^{n+}]}$$

$$E = E^\circ - \frac{RT}{nF}\ln\left(\frac{[M]}{[M^+]}\right) - \frac{RT}{nF}\ln(K_{ox}) - \frac{RT}{nF}\ln(a_X)$$

When ion-pairing occurs in the reduced state (anion) and not in the oxidized state (neutral) the reduction potential varies as $+\ln(a_X)$ [1].

$$X^+ + M^- \rightleftharpoons (X\cdot M)K_{red} = \frac{\gamma[(X\cdot M)]}{\gamma_x[X^+]\gamma_+[M^{n+}]}$$

$$E = E^\circ - \frac{RT}{nF}\ln\left(\frac{[M^-]}{[M]}\right) + \frac{RT}{nF}\ln(K_{red}) + \frac{RT}{nF}\ln(a_X)$$

Where ion-pair equilibria are involved in both ions of a redox couple, differing in charge and pairing with a monoanion, the reduction potential varies as $2ART/2.303nF$, where $A = 0.509$ or 60 mV per ionic strength unit.

$$X^- + M^{n+} \rightleftharpoons (X\cdot M)^{n-1}K_{ox} = \frac{\gamma_{(n-1)}[X\cdot M)^{n-1}]}{\gamma_x[X^-]\gamma_n[M^{n+}]}$$

$$X^- + M^{(n-1)+} \rightleftharpoons (X\cdot M)^{(n-1)}K_{red}$$
$$= \frac{\gamma_{(n-2)}[(X\cdot M)^{n-2}]}{\gamma_x[X^-]\gamma_{(n-1)}[M^{(n-1)+}]}$$

$$E = E^\circ - \frac{RT}{nF}\ln\left(\frac{[M^{(n-1)+}]}{[M^{n+}]}\right)$$

$$E = E^\circ - \frac{RT}{nF}\ln\left(\frac{[(X\cdot M)^{n-2}]}{[X\cdot M)^{n-1}]}\right) - \frac{RT}{nF}\ln\left(\frac{K_{ox}}{K_{red}}\right)$$
$$- \frac{RT}{nF}\ln\left(\frac{\gamma_n\gamma_{(n-2)}}{\gamma_{(n-1)}\gamma_{(n-1)}}\right)$$

but, $\log(\gamma) = -Az_i^2\sqrt{\mu}$, where $A = 0.509$ in aqueous solution. Consequently, the last term can be expressed as

$$\log\left(\frac{\gamma_n\gamma_{(n-2)}}{\gamma_{(n-1)}\gamma_{(n-1)}}\right)$$
$$= \log\gamma_n + \log\gamma_{(n-2)} - \log\gamma_{(n-1)} - \log\gamma_{(n-1)}$$
$$= -0.509\{n^2 + (n-2)^2 - 2(n-1)^2\}\sqrt{\mu}$$
$$= -0.509\{n^2 + n^2 - 4n + 4 - 2n^2 + 4n - 2\}\sqrt{\mu}$$
$$= -0.509(4-2) = -1.018\sqrt{\mu}$$

$$\therefore E = E^\circ - 0.059\left\{\log\left(\frac{[(X\cdot M)^{n-2}]}{[(X\cdot M)^{n-1}]}\right) - \log\left(\frac{K_{ox}}{K_{red}}\right)\right\} + 0.060\sqrt{\mu}$$

$$E = E^{\circ\prime} - 0.059\log\left(\frac{[(X\cdot M)^{n-2}]}{[(X\cdot M)^{n-1}]}\right) + 0.060\sqrt{\mu},$$

where

$$E^{\circ\prime} = E^\circ - 0.059\log\left(\frac{K_{ox}}{K_{red}}\right)$$

If the charge on M is negative and it pairs with a cation, then

$$X^+ + M^{n-} \rightleftharpoons (X\cdot M)^{(n-1)-}K_{ox} = \frac{\gamma_{(n-1)}[(X\cdot M)^{(n-1)-}]}{\gamma_x[X^+]\gamma_n[M^{n-}]}$$

$$X^+ + M^{(n+1)-} \rightleftharpoons (X\cdot M)^{n-}$$

$$K_{red} = \frac{\gamma_n[(X\cdot M)^{n-}]}{\gamma_x[X^+]\gamma_{(n+1)}[M^{(n+1)-}]}$$

$$E = E^\circ - \frac{RT}{nF}\ln\left(\frac{[M^{(n+1)-}]}{[M^{n-}]}\right)$$

$$E = E^\circ - \frac{RT}{nF}\ln\left(\frac{[(X\cdot M)^{n-}]}{[(X\cdot M)^{n-1)-}]}\right) - \frac{RT}{nF}\ln\left(\frac{K_{ox}}{K_{red}}\right)$$
$$- \frac{RT}{nF}\ln\left(\frac{\gamma_n\gamma_n}{\gamma_{(n-1)}\gamma_{(n+1)}}\right)$$

but,

$$\log\left(\frac{\gamma_n \gamma_n}{\gamma_{(n-1)}\gamma_{(n+1)}}\right) = \log \gamma_n + \log \gamma_n - \log \gamma_{(n-1)} + \log \gamma_{(n+1)}$$

$$= -0.509\{2n^2-(n-1)^2-(n+1)^2\}\sqrt{\mu}$$

$$= -0.509\{2n^2-n^2+2n-1-n^2-2n-1\}\sqrt{\mu}$$

$$= -0.509(-2) = +1.018\sqrt{\mu}$$

$$E = E^\circ - \frac{RT}{nF}\ln\left(\frac{[(X\cdot M)^{n-}]}{[(X\cdot M)^{(n-1)-}]}\right) - \frac{RT}{nF}\ln\left(\frac{K_{ox}}{K_{red}}\right) - 0.60\sqrt{\mu}$$

Reference

A1 J. T. Hupp, *J. Am. Chem. Soc.*, *29* (1990) 5010–5012.